Viscous flows down an inclined plane from point and line sources

By JOHN R. LISTER

Institute of Theoretical Geophysics, Department of Applied Mathematics and Theoretical
Physics, University of Cambridge, Silver Street, Cambridge CB3 9EW, UK

The flow of a viscous fluid from a point or line source on an inclined plane is analysed using the equations of lubrication theory in which surface tension is neglected. At short times, when the gradient of the interfacial thickness is much greater than that of the plane, the fluid is shown to spread symmetrically from the source, as on a horizontal plane. At long times, the flow is predominantly downslope, with some cross-slope spreading for the case of a point source. Similarity solutions for the long-time behaviour of the governing nonlinear partial differential equations are found for the case in which the volume of fluid increases with time like t^α, where α is a constant. The two-dimensional equations appropriate to a line source are hyperbolic in the self-similar regime and the similarity profile is found analytically to end abruptly at a downslope position which increases like $t^{(2\alpha+1)/3}$. Inclusion of higher-order terms in the analysis resolves this frontal shock into a boundary-layer structure of width comparable to the thickness of the current. Owing to the term representing cross-slope spreading, the mathematical structure of the equations is considerably more complex for flow from a point source and the similarity form is found numerically in this case. Though the downslope and cross-slope extents of the current again increase with time according to a power-law if $\alpha > 0$, they also depend on a power of $\ln t$ if $\alpha = 0$. The leading-order near-source structure is shown to be that of steady flow from a constant-flux source of strength given by the instantaneous flow rate. For sources with $\alpha > 1$, the contact line advances at all points on the perimeter of the flow and the entire plane is eventually covered by the flow; for sources with $0 < \alpha < 1$, only a portion of the contact line is advancing at any time and only that part of the plane with $|y| \leqslant cx^{3\alpha/(4\alpha+3)}$ is eventually covered, where x and y are the downslope and cross-slope coordinates and c is a constant. The theoretical spreading relationships and planforms are found to be in good agreement with experimental measurements of constant-volume and constant-flux flows of viscous fluids from a point source on a plane. At very long times, however, the experimental flows are observed to be unstable to the formation of a capillary rivulet at the nose of the current.

1. Introduction

The buoyancy-driven flow of a dense fluid over a rigid boundary is a well studied and important fluid-mechanical problem with many applications. While much of the early work focused on the large-Reynolds-number gravity currents found at the boundaries of the Earth's oceans, atmosphere and lakes, more attention has been paid recently to the viscous gravity currents relevant to geological applications and to a range of industrial processes. In this paper we present similarity solutions for the fundamental problem of a viscous gravity current generated by a point or line source

of fluid on an inclined plane. We consider flows with volumes proportional to t^α, thus including the important cases of fixed-volume ($\alpha = 0$) and fixed-flux ($\alpha = 1$) release.

The present analysis extends a number of previously published results. Schwartz & Michaelides (1988) described a numerical simulation of a flow on an inclined plane with constant injection through a finite circular hole. Huppert (1982a) found similarity solutions for the spread of a viscous fluid of volume proportional to t^α over a rigid horizontal plane in both axisymmetric and two-dimensional geometries. We show below that these solutions also represent the short-time behaviour of flows on an inclined plane. We focus, therefore, on the unstudied long-time behaviour for which the slope of the plane provides the dominant contribution to the buoyancy and there is strong asymmetry between the upslope and downslope directions. For the case of a point source of fluid, it is found that the near-source behaviour is given at leading order by Smith's (1973) solution for steady flow on an inclined plane from a constant-flux source, but evaluated at the instantaneous rate of efflux. Higher-order corrections arise from the variation in the source flux ($\alpha \neq 1$) and the finite downstream extent of a current that started at $t = 0$.

Though Huppert's (1982a) solutions neglected the contact-line effects and capillary forces at the nose of the current, they were found to be in excellent agreement with experimental observations, thus demonstrating that the details of the nose condition did not matter and that the spread was governed by a simple global balance between buoyancy and viscous forces. It was also found that, for the case of point release, the flow rapidly approached a stable axiysmmetric planform. A different behaviour was observed by Huppert (1982b) for the two-dimensional flow of a fixed volume of fluid on an inclined plane. The initial behaviour was again well described by a solution based on a viscous–buoyancy balance. However, at a critical distance downslope from the line of release, the previously straight front of the current developed a capillary instability with a characteristic cross-slope wavelength. This instability grew rapidly so that the downslope flow was eventually concentrated in fingers or rivulets extending down the plane from near the location of the onset of instability.

Despite further experimental, theoretical and numerical studies (Silvi & Dussan V. 1985; Troian et al. 1989; Schwartz 1989; Hocking 1990), a theoretical instability criterion that is fully consistent with the experimental observations of both the onset and the wavelength of the instability has not yet emerged. This may be attributed, at least in part, to the difficulty of adequately modelling a moving contact line. Interestingly, a number of different models of the contact line (Troian et al. 1989; Hocking 1990; Goodwin & Homsy 1991) all predict a small capillary bulge immediately behind the undeformed front. It thus seems likely that the instability is driven by cross-slope gradients in capillary pressure, induced by variations in the thickness of this bulge, in a manner analogous to the capillary breakup of a liquid jet.

In §§2–4 we present a theoretical description of flow from point and line sources on a plane based only on a viscous–buoyancy balance. Inertial and surface-tension forces are assumed to be negligible everywhere, as are the effects of diffusion or mixing at the fluid interface. Except possibly at very early times, the extent of the flow will be much greater than its thickness, suggesting the use of lubrication theory. The problem is defined and the basic equations derived in §2. These equations are solved analytically for the case of a line source, allowing the frontal and near-source structure of the solutions to be determined in §3. The insight derived from these two-dimensional solutions is used in §4 to discuss the case of a point-source release for

which analytic solution is not possible except in the case $\alpha = 0$ and the equations must be solved numerically.

Formally, the neglect of surface tension and contact-line effects in the theory will be valid if the Bond number $B = \rho g L^2/\sigma \gg 1$, where ρ is the density, g is the acceleration due to gravity, L is the cross-slope lengthscale of the current and σ is the coefficient of surface tension. As described in §5, the theoretical predictions are found to be in very good agreement with experimental observations of lengths, widths and shapes of fixed-flux and fixed-volume currents from a point source. At very long times, however, when the current is thin and slowly moving, interfacial effects start to play a role. A capillary rivulet, similar to those described by Huppert (1982 *b*), is observed to form at the nose of the current and channels the flow downslope, inhibiting further cross-slope spreading. We conclude that the main evolution of the flow is well described, as in Huppert (1982 *a*), by a simple viscous–buoyancy balance, but that the flow ultimately becomes unstable at some critical distance downslope.

2. Lubrication equations and scaling

Suppose a fluid of constant density ρ and viscosity μ is released onto a plane inclined at an angle θ to the horizontal. Let x denote the downslope coordinate measured from the point or line of release, y the cross-slope coordinate, z the coordinate normal to the plane and $h(x, y)$ the depth of the fluid layer. After a sufficient length of time the extent of the flow will be much greater than its thickness and hence we assume that $|\nabla h| \ll 1$, where ∇ denotes the gradient operator in the (x, y)-plane. The effects of inertia and surface tension are assumed to be negligible. From these assumptions it follows that the fluid pressure and velocity are given by†

$$p = \rho g\{(h - z)\cos\theta - x\sin\theta\}, \tag{2.1}$$

$$\boldsymbol{u} = -\frac{1}{2\mu} z(2h - z)\,\nabla p. \tag{2.2}$$

We substitute into the depth-averaged equation of continuity for the flow to obtain

$$\frac{\partial h}{\partial t} = \frac{\rho g \sin\theta}{3\mu} \left\{ \cot\theta \frac{\partial}{\partial y}\left(h^3 \frac{\partial h}{\partial y}\right) + \cot\theta \frac{\partial}{\partial x}\left(h^3 \frac{\partial h}{\partial x}\right) - \frac{\partial h^3}{\partial x} \right\}. \tag{2.3}$$

It should be noted that, since we have assumed $|\nabla h| \ll 1$, we also require $\tan\theta \ll 1$ if the second term on the right-hand side of (2.3) is to be comparable with the third.

We consider point and line sources of fluid of strength such that the volume released onto the plane is proportional to t^α ($t \geqslant 0$), where $\alpha \geqslant 0$. Thus we look for solutions of (2.3) subject to the volume constraint

$$\int_{x_{\mathrm{T}}}^{x_{\mathrm{N}}} \int_{-y_{\mathrm{P}}(x)}^{y_{\mathrm{P}}(x)} h \, \mathrm{d}y \, \mathrm{d}x = Q t^\alpha \quad \text{(point source),} \tag{2.4}$$

$$\int_{x_{\mathrm{T}}}^{x_{\mathrm{N}}} h \, \mathrm{d}x = q t^\alpha \quad \text{(line source),} \tag{2.5}$$

where the perimeter of the flow is given by $|y| = y_{\mathrm{P}}(x, t)$ in $x_{\mathrm{T}}(t) < x < x_{\mathrm{N}}(t)$ for a point

† As shown by Huppert (1982 *a*), a current under a deep layer of overlying fluid of density $\rho_{\mathrm{a}} < \rho$ may be described by the above analysis with g replaced by $g' = g(\rho - \rho_{\mathrm{a}})/\rho$, since the stress exerted by the ambient fluid on the flow is negligible.

source, and the (two-dimensional) flow lies in $x_T(t) < x < x_N(t)$ for a line source. For later comparison with experimental measurements we define $y_M(t)$ to be the maximum value of $y_P(x, t)$ at time t.

We define dimensionless variables $T = t/T^*$, $X = x/X^*$, $Y = y/Y^*$ and $H = h/H^*$, where

$$T^* = \left(\frac{c_\theta^5}{QR^3}\right)^{1/(\alpha+3)}, \quad X^* = Y^* = H^* c_\theta = \left(\frac{Q c_\theta^{2\alpha+1}}{R^\alpha}\right)^{1/(\alpha+3)} \quad \text{(point source)}, \quad (2.6)$$

$$T^* = \left(\frac{c_\theta^3}{qR^2}\right)^{1/(\alpha+2)}, \quad X^* = H^* c_\theta = \left(\frac{q c_\theta^{2\alpha+1}}{R^\alpha}\right)^{1/(\alpha+2)} \quad \text{(line source)}, \quad (2.7)$$

$c_\theta = \cot\theta$ and $R = \rho g \sin\theta / 3\mu$. Expressed in the dimensionless variables, (2.3)–(2.5) reduce to the forms

$$\frac{\partial H}{\partial T} = \frac{\partial}{\partial Y}\left(H^3 \frac{\partial H}{\partial Y}\right) + \frac{\partial}{\partial X}\left(H^3 \frac{\partial H}{\partial X}\right) - \frac{\partial H^3}{\partial X}, \quad \int_{X_T}^{X_N} \int_{-Y_P(X)}^{Y_P(X)} H \, dY \, dX = T^\alpha \quad \text{(point source)},$$

$$(2.8a,b)$$

$$\frac{\partial H}{\partial T} = \frac{\partial}{\partial X}\left(H^3 \frac{\partial H}{\partial X}\right) - \frac{\partial H^3}{\partial X}, \quad \int_{X_T}^{X_N} H \, dX = T^\alpha \quad \text{(line source)}, \quad (2.9a,b)$$

Since α is the only dimensionless parameter in (2.8) and (2.9), this scaling shows the universality of the evolution of all flows with a given value of α and $0 < \theta \ll 1$.

By looking for possible asymptotic balances, (2.8) and (2.9) can be rescaled again to show the behaviour at early and late times. For example, in order to consider $t \ll T^*$ for a point source, we define dimensionless variables $\hat{T}, \hat{X}, \hat{Y}$ and $\hat{H}$ using the scales λT^*, $\lambda^{(3\alpha+1)/8} X^*$, $\lambda^{(3\alpha+1)/8} Y^*$ and $\lambda^{(\alpha-1)/4} H^*$, where $\lambda \ll 1$, instead of those given by (2.6). We find that

$$\frac{\partial \hat{H}}{\partial \hat{T}} = \hat{\mathbf{\nabla}} \cdot (\hat{H}^3 \hat{\mathbf{\nabla}} \hat{H}) + O(\lambda^{(\alpha+3)/8}) \quad \text{(point source, early times, } \lambda \ll 1), \quad (2.10a)$$

with the form of the volume constraint (2.8b) unaltered. Similarly, in order to consider $t \gg T^*$, we use scales ΛT^*, $\Lambda^{(4\alpha+3)/9} X^*$, $\Lambda^{\alpha/3} Y^*$ and $\Lambda^{(2\alpha-3)/9} H^*$, where $\Lambda \gg 1$, to obtain

$$\frac{\partial \hat{H}}{\partial \hat{T}} = \frac{\partial}{\partial \hat{Y}}\left(\hat{H}^3 \frac{\partial \hat{H}}{\partial \hat{Y}}\right) - \frac{\partial \hat{H}^3}{\partial \hat{X}} + O(\Lambda^{-(2\alpha+3)/9}) \quad \text{(point source, late times, } \Lambda \gg 1).$$

$$(2.10b)$$

The early- and late-time solutions for a line source are found by the scalings λT^*, $\lambda^{(3\alpha+1)/5} X^*$ and $\lambda^{(2\alpha-1)/5} H^*$, where $\lambda \ll 1$ and

$$\frac{\partial \hat{H}}{\partial \hat{T}} = \frac{\partial}{\partial \hat{X}}\left(\hat{H}^3 \frac{\partial \hat{H}}{\partial \hat{X}}\right) + O(\lambda^{(\alpha+2)/5}) \quad \text{(line source, early times, } \lambda \ll 1). \quad (2.11a)$$

or by the scalings ΛT^*, $\Lambda^{(2\alpha+1)/3} X^*$ and $\Lambda^{(\alpha-1)/3} H^*$, where $\Lambda \gg 1$ and

$$\frac{\partial \hat{H}}{\partial \hat{T}} = -\frac{\partial \hat{H}^3}{\partial \hat{X}} + O(\Lambda^{-(\alpha+2)/3}) \quad \text{(line source, late times, } \Lambda \gg 1). \quad (2.11b)$$

These rescalings are illuminating for three reasons. Firstly, solutions of the limiting forms of (2.10) and (2.11) as $\lambda \to 0$ or $\Lambda \to \infty$ represent similarity solutions for the early- and late-time behaviour. The asymptotic dependence of the dimensions of
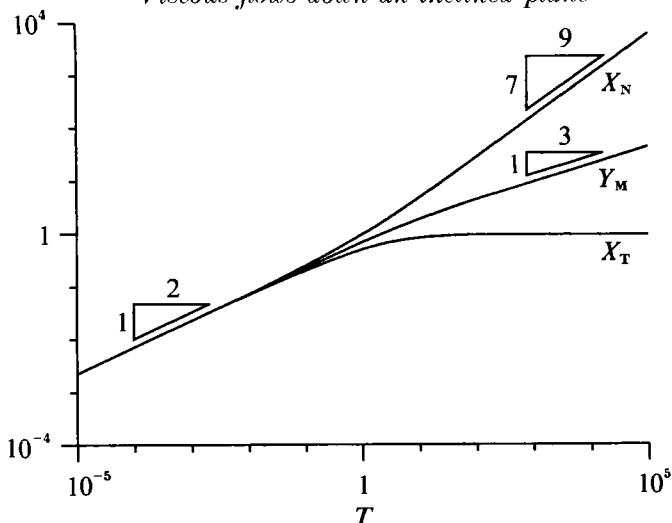
FIGURE 1. The development of the downslope extent X_N, the upslope extent X_T and the cross-slope extent Y_M with time for a fixed-flux release on an inclined plane. Initial axisymmetric spreading proportional to $T^{1/2}$ gives way to predominantly downslope flow when $T = O(1)$. The dimensionless variables are defined using the scalings (2.6).

Source	Limit	Downslope extent x	Cross-slope extent y	Thickness h
Point	$t \ll T^*$	$\sim (Q^3 \bar{R} \cos\theta\, t^{3\alpha+1})^{\frac{1}{8}}$	$\sim (Q^3 \bar{R} \cos\theta\, t^{3\alpha+1})^{\frac{1}{8}}$	$\sim \left(\dfrac{Q t^{\alpha-1}}{\bar{R}\cos\theta)} \right)^{\frac{1}{4}}$
Point	$t \gg T^*$	$\sim \left(\dfrac{Q^4 \bar{R}^3 \sin^5\theta\, t^{4\alpha+3}}{\cos^2\theta} \right)^{\frac{1}{9}}$	$\sim \left(\dfrac{Q\cos\theta\, t^\alpha}{\sin\theta} \right)^{\frac{1}{3}}$	$\sim \left(\dfrac{Q^2 t^{2\alpha-3}}{\bar{R}^3 \cos\theta \sin^2\theta} \right)^{\frac{1}{9}}$
Line	$t \ll T^*$	$\sim (Q^3 \bar{R} \cos\theta\, t^{3\alpha+1})^{\frac{1}{5}}$	—	$\sim \left(\dfrac{Q^2 t^{2\alpha-1}}{\bar{R}\cos\theta} \right)^{\frac{1}{5}}$
Line	$t \gg T^*$	$\sim (Q^2 \bar{R} \sin\theta\, t^{2\alpha+1})^{\frac{1}{3}}$	—	$\sim \left(\dfrac{Q t^{\alpha-1}}{\bar{R}\sin\theta} \right)^{\frac{1}{3}}$

TABLE 1. Asymptotic scalings for the dimensions of a viscous gravity current on an inclined plane. The value of T^* is defined by (2.6) or (2.7), and $\bar{R} = g'/3\nu$ where g' denotes the reduced gravity and ν the kinematic viscosity. The results for $t \ll T^*$ reduce to those of Huppert (1982a) when $\cos\theta = 1$. As described in §4.4, when $\alpha = 0$ the long-time scalings for a point source need to be modified by terms involving $\ln(t/T^*)$.

the current is then readily deduced from the scalings used to derive the similarity form. For example, the self-similar scaling with respect to ΛT^* and $\Lambda^{(2\alpha+1)/3}X^*$ for a line source at late times shows that $x_N/X^* \sim (t/T^*)^{(2\alpha+1)/3}$. The dimensional form of these results is summarized in table 1. Secondly, it may be seen that there is a transition when $t = O(T^*)$, or $T = O(1)$, from a regime in which $\partial h/\partial x \gg \tan\theta$ (equivalently $\partial H/\partial X \gg 1$) and the spreading current is unaffected by the slope to a regime in which $\partial h/\partial x \ll \tan\theta$ (equivalently $\partial H/\partial X \ll 1$) and current flows dominantly downslope; X^*, Y^* and H^* are the typical dimensions of the current at the time of transition. This transition may be seen, for example, in the computed evolution of $X_N(T)$ and $Y_M(T)$ for $\alpha = 1$ shown in figure 1. It may be noted that the early-time behaviour can only be described by the lubrication approximation

if $\tan \theta \ll 1$, but that the long-time behaviour will always eventually lie in the lubrication regime. Thirdly, the limiting forms of (2.10*a*) and (2.11*a*) show that the early-time behaviour is given by the solution for the spread of a gravity current on a horizontal plane derived by Huppert (1982*a*). Therefore, we shall now focus on the unstudied intermediate- and long-time behaviour.

In order to obtain the approach to the long-time similarity solution, we first define $s = \ln T$. For the case of a point source we then substitute $\xi = XT^{-(4\alpha+3)/9}$, $\eta = YT^{-\alpha/3}$ and $\phi(s, \xi, \eta) = HT^{-(2\alpha-3)/9}$ into (2.8*a*) to obtain

$$\phi_s + \alpha \phi = \left(\frac{4\alpha + 3}{9} \xi \phi - \phi^3 \right)_\xi + \left(\frac{\alpha}{3} \eta \phi + \phi^3 \phi_\eta \right)_\eta + \mathrm{e}^{-2(\alpha+3)s/9} (\phi^3 \phi_\xi)_\xi, \qquad (2.12)$$

where subscripts denote differentiation. For a line source, we substitute $\xi = XT^{-(2\alpha+1)/3}$ and $\phi(s, \xi) = HT^{-(\alpha-1)/3}$ into (2.9*a*) to obtain

$$\phi_s + \alpha \phi = \left(\frac{2\alpha + 1}{3} \xi \phi - \phi^3 \right)_\xi + \mathrm{e}^{-(\alpha+2)s/3} (\phi^3 \phi_\xi)_\xi, \qquad (2.13)$$

In both cases, the source at $X = 0$ corresponds to a volume influx at $\xi = 0$ of constant strength α, and the volume constraints (2.8*b*) and (2.9*b*) become $\int \phi = 1$. The long-time similarity solutions are given by equating ϕ_s and the exponentially small terms to zero in (2.12) and (2.13). These solutions may be found numerically by retaining the term ϕ_s and integrating with respect to s until a steady state is attained.

3. Line sources

The long-time solution for a line source may be determined analytically. This is particularly welcome since the structure of the solution obtained offers valuable insight into the more complicated problem of a point source for which analytic solution is not possible except in the case $\alpha = 0$.

3.1. *The long-time similarity solution*

The long-time similarity solution of (2.13) satisfies

$$\alpha \phi = \frac{\mathrm{d}}{\mathrm{d}\xi} \left(\frac{2\alpha + 1}{3} \xi \phi - \phi^3 \right). \qquad (3.1)$$

This equation may be integrated using the integrating factor $\phi^{3\alpha/(1-\alpha)}$ to obtain an implicit expression for the similarity profile

$$\xi = 3 \left(\frac{\phi^{3/(1-\alpha)} - \phi_0^{3/(1-\alpha)}}{\phi^{(1+2\alpha)/(1-\alpha)}} \right), \qquad (3.2)$$

where $\phi_0 = \phi(0)$. From (3.1) the limit of the downslope flux as $\xi \to 0_+$ is ϕ_0^3 and hence $\phi_0 = \alpha^{\frac{1}{3}}$. The location ξ_N and height ϕ_N of the nose are determined by the volume constraint, $\int \phi = 1$, to be

$$\xi_N = \frac{3}{2\phi_0} \left(\frac{2\alpha}{1+2\alpha} \right)^{(1+2\alpha)/3}, \quad \phi_N = \left(\frac{1+2\alpha}{2\alpha} \right)^{(1-\alpha)/3} \phi_0. \qquad (3.3\,a,b)$$

A fixed-volume release is described by

$$\phi = (\tfrac{1}{3}\xi)^{\frac{1}{2}}, \quad \xi_N = 3/2^{\frac{2}{3}}, \quad \phi_N = 2^{-\frac{1}{3}} \quad (\alpha = 0), \qquad (3.4)$$
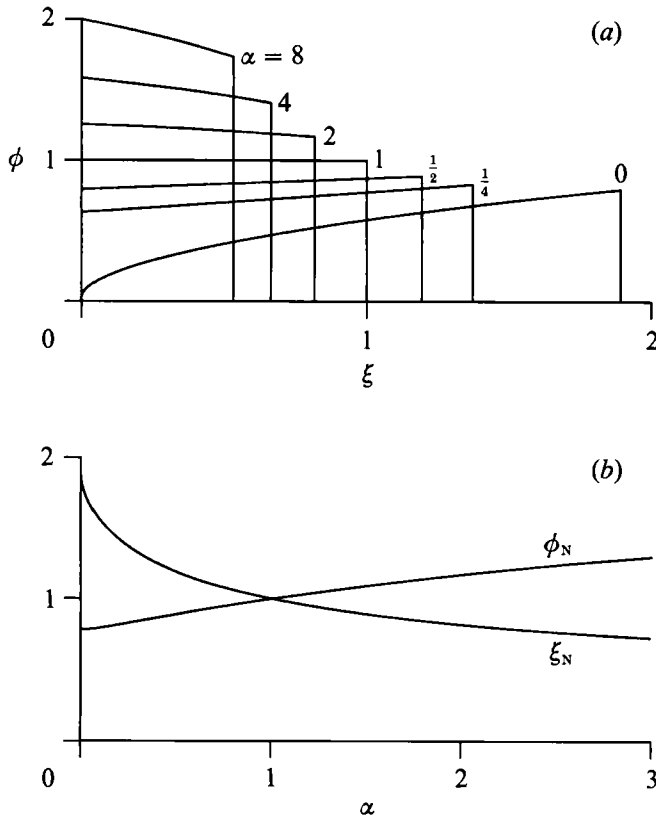
FIGURE 2. (a) The similarity solution (3.2) for the thickness of a two-dimensional flow with volume proportional to t^α for a number of values of α, which is fed from a line source on an inclined plane. (b) The similarity constants (3.3) for a line source as functions of α.

as shown by Huppert (1982b), and a fixed-flux release approaches the simple form

$$\phi = 1, \quad \xi_N = 1, \quad \phi_N = 1 \quad (\alpha = 1). \tag{3.5}$$

Solutions for other values of α are shown in figure 2.

3.2. *The structure at the source and nose*

It will be noticed that the similarity solution (3.2) ends abruptly at $\xi = 0$ (unless $\alpha = 0$) and at $\xi = \xi_N$. Mathematically, this behaviour reflects the fact that the limit $s \to \infty$ is a singular perturbation of (2.13) caused by the loss of the highest ξ-derivative. Physically, the discontinuous profile may need to be resolved by the inclusion of surface tension (Huppert 1982b; Troian *et al.* 1989; Hocking 1990) or by the abandonment of lubrication theory where $|\nabla h| \not\ll 1$ (Goodwin & Homsy 1991). However, the experimental results of Huppert (1982a, b) indicate that, provided the flow dos not become unstable, the breakdown of the viscous–buoyancy balance or of the lubrication approximation in a small neighbourhood of the contact line does not affect the self-similar structure of the majority of the flow or the global spreading rate.

If $\tan \theta \ll 1$ and $B \gg 1$ the details of the flow near the contact lines are still described to leading order by the simple viscous–buoyancy balance expressed by
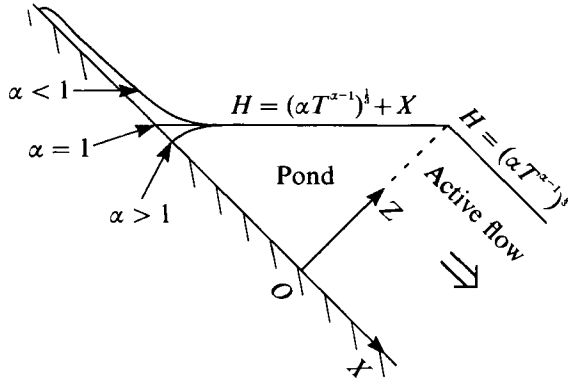
FIGURE 3. The structure of the two-dimensional flow near a line source at O on an inclined plane. Downslope from the source the flow is given by the similarity solution (3.2). Upslope from the source is a nearly stagnant pond of fluid with horizontal upper surface. The pond slowly increases in depth ($\alpha > 1$) or is fed by a draining film from a previous 'high-water' level ($\alpha < 1$).

(2.9a). An asymptotic analysis for the case $\alpha = 0$ is given by Grundy (1983). For the general case, we resolve the frontal shock by the boundary-layer scaling $\chi = (\xi_N - \xi)\,e^{(\alpha+2)s/3}$ with respect to which the leading-order terms as $\xi \to \xi_N$ are

$$\tfrac{1}{3}(2\alpha+1)\,\xi_N\,\phi_\chi - 3\phi^2\phi_\chi = (\phi^3\phi_\chi)_\chi. \tag{3.6}$$

This equation can be integrated from $\phi = 0$ at $\chi = 0$ to obtain

$$\chi = \tfrac{1}{2}\phi_N \ln\!\left(\frac{\phi_N+\phi}{\phi_N-\phi}\right) - \phi, \tag{3.7}$$

where $\phi_N = \{\tfrac{1}{3}(2\alpha+1)\xi_N\}^{\frac{1}{2}}$. Equation (3.7) implies that $\phi \to \phi_N$ as $\chi \to \infty$. Thus the condition of matching between the boundary-layer solution and (3.2) is that the limiting value ϕ_N given in this section should be the same as that given by (3.3b). This condition is satisfied for the value of ξ_N given by (3.3a). It may be shown that this ability to match a frontal boundary-layer structure to the main flow follows from the structure of (3.1) and the constraint on the total volume.

As noted above, if $\alpha > 0$ there is also a backwards-facing discontinuity at $\xi = 0$ which is resolved by a boundary-layer structure.† The leading-order solution is a flat nearly-stagnant pond $H(X,T) = \alpha^{\frac{1}{3}}T^{(\alpha-1)/3} + X$ (or in similarity variables $\phi = \alpha^{\frac{1}{3}} + \xi\,e^{(\alpha+2)s/3}$) lying upstream from the source (figure 3). This pond is either filling slowly or emptying slowly, depending on whether $H(0, T)$ is increasing or decreasing or, equivalently, whether α is greater than or less than 1. Thus, in a formal expansion of the solution of (2.13), the solution for a flat pond would itself need to be matched either to an advancing contact line at $X = X_T$ ($\alpha > 1$) or to a thin film which drains fluid from the previous 'high-water mark' into the pond ($\alpha < 1$).

Finally we note that $\phi \propto \chi^{\frac{1}{3}}$ as $\chi \to 0$ in (3.6), showing that, even if $\tan\theta \ll 1$, the lubrication approximation used here must break down in a subdomain of the frontal structure (see Goodwin & Homsy 1991). Here again we note the experimental observation that the breakdown of our analysis in the immediate vicinity of the contact line has a negligible effect on the predicted flow (Huppert 1982a, b).

† If $\alpha = 0$ the square-root singularity at $\xi = 0$ in (3.4a) may be resolved in a similar manner (Grundy 1983).

4. Point sources

The long-time structure of flow from a point source is considerably more complicated than that from a line source. Some useful results can be derived by asymptotic analysis of the flow near the source and near the contact line $\eta_P(\xi)$. These are discussed briefly below, omitting much of the mathematical detail for simplicity. However, except in the case $\alpha = 0$, the solutions of the nonlinear partial differential equations must ultimately be determined numerically by a scheme such as that described in Appendix A.

4.1. *The near-source structure* $(\alpha \neq 0)$

Owing to the diffusive terms in (2.8a), changes in the source flux and in the location of the contact line are immediately felt throughout the flow. Nevertheless, we expect that changes in the flow close to the source will be dominated by the effects of changes in the value of the source flux. By seeking a balance between the three terms on the right-hand side of (2.8a) and the instantaneous flux $\alpha T^{\alpha-1}$, we are motivated to rescale the equations by defining $\mathcal{H} = H/L$, $\mathcal{X} = X/L$ and $\mathcal{Y} = Y/L$, where $L = (\alpha T^{\alpha-1})^{\frac{1}{4}}$. Assuming that $\mathcal{H}$, $\mathcal{X}$ and $\mathcal{Y}$ are $O(1)$, we find that

$$\frac{\partial}{\partial \mathcal{Y}}\left(\mathcal{H}^3 \frac{\partial \mathcal{H}}{\partial \mathcal{Y}}\right) + \frac{\partial}{\partial \mathcal{X}}\left(\mathcal{H}^3 \frac{\partial \mathcal{H}}{\partial \mathcal{X}}\right) - \frac{\partial \mathcal{H}^3}{\partial \mathcal{X}} = O(T^{-(3+\alpha)/4}) \tag{4.1}$$

and that the source strength has now been scaled to unity. Thus with these scalings the near-source flow is seen to approach a steady structure, which is independent of α. A numerical solution of (4.1) is shown in figure 4.†

It may be noted that the solution of (4.1) is a quasi-steady approximation of the near-source solution of (2.8). As with the quasi-steady flat pond lying upslope from the line source in the solution of (2.9), the solution of (4.1) needs to be matched either to a slowly advancing contact line ($\alpha > 1$) or to a thin film which drains fluid from previously wetted areas of the plane ($\alpha < 1$). In the case $\alpha \geqslant 1$ figure 4 shows that the limit of upslope flow is given by $X_T \sim 0.92 T^{(\alpha-1)/4}$. In the case $\alpha < 1$ the limit of upslope flow is attained when $T = O(1)$ and is constant thereafter.

As $\mathcal{X} \to \infty$, the solution of (4.1) asymptotes to the similarity solution given by Smith (1973) for the steady flow far downstream of a constant-flux source. In this regime (4.1) and the source-flux condition can be approximated as

$$\frac{\partial}{\partial \mathcal{Y}}\left(\mathcal{H}^3 \frac{\partial \mathcal{H}}{\partial \mathcal{Y}}\right) = \frac{\partial \mathcal{H}^3}{\partial \mathcal{X}}, \quad \int_{-\mathcal{Y}_P}^{\mathcal{Y}_P} \mathcal{H}^3 \, \mathrm{d}\mathcal{Y} = 1 \quad (\mathcal{X} \gg 1), \tag{4.2}$$

with errors of order $\mathcal{X}^{-\frac{8}{7}}$. It is readily shown that the similarity solution of (4.2) is given by

$$\mathcal{H} = \tfrac{3}{14}\mathcal{X}^{-\frac{1}{7}}\left\{P^2 - \frac{\mathcal{Y}^2}{\mathcal{X}^{\frac{6}{7}}}\right\}, \tag{4.3}$$

where $P = (12005/108)^{\frac{1}{7}}$, as was first derived and verified experimentally by Smith (1973). Comparison of the scalings used to derive (4.1) with those used to derive (2.12) shows that (4.2) and (4.3) give the leading-order behaviour of (2.8) in the region $\xi \ll 1$ and $\mathcal{X} \gg 1$. Expressed in the unscaled variables, the solution of (2.8) is described by (4.3) in the region $T^{(\alpha-1)/4} \ll X \ll T^{(4\alpha+3)/9}$; the term $(H^3 H_X)_X$ cannot be neglected in $X = O(T^{(\alpha-1)/4})$ and the term H_T cannot be neglected in $X = O(T^{(4\alpha+3)/9})$ (see figure 5).

† As $\mathcal{X}$, $\mathcal{Y} \to 0$, $\mathcal{H} \sim |\ln \mathcal{R}|^{\frac{1}{4}}$, where $\mathcal{R}^2 = \mathcal{X}^2 + \mathcal{Y}^2$. Thus the lubrication approximation breaks down in a subdomain near the source of radius $\mathcal{R} \sim \tan\theta/|\ln\tan\theta|^{\frac{1}{4}} \ll 1$.)
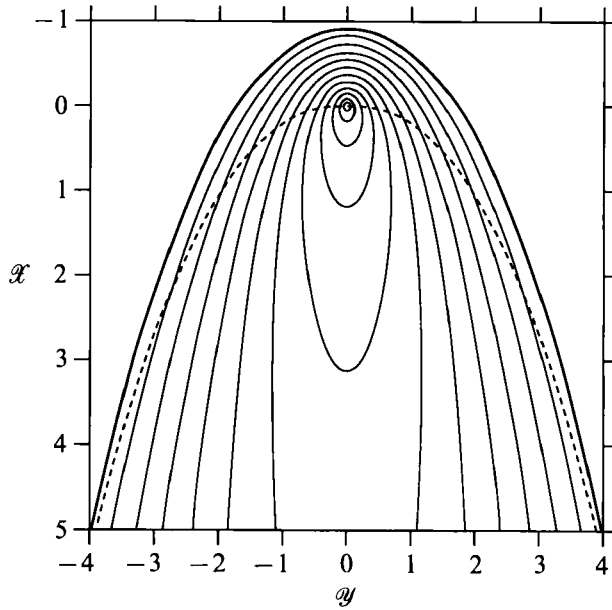
FIGURE 4. The quasi-steady near-source solution (4.1) for flow from a point source on an inclined plane. The dashed line represents the limiting form $\mathcal{Y} = (12005\mathcal{X}^3/108)^{1/7}$ for the perimeter of the flow as $\mathcal{X} \to \infty$.
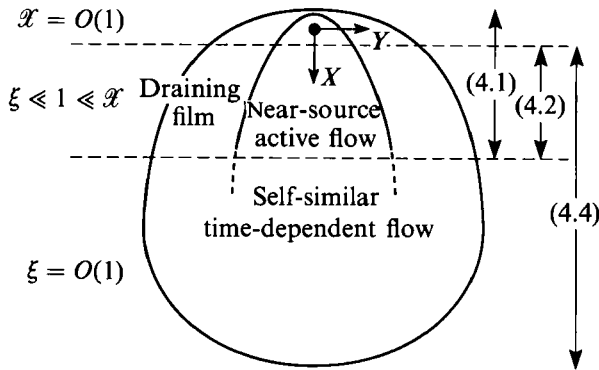

FIGURE 5. The asymptotic similarity structure for a flow of volume T^α from a point source, for the case $0 < \alpha < 1$. The figure shows the regions of validity of (4.1)–(4.4), where the scalings of the downslope distance X are defined by $\xi = XT^{-(4\alpha+3)/9}$ and $\mathcal{X} = X(\alpha T^{\alpha-1})^{-1/4}$. In $\xi \ll 1 \ll \mathcal{X}$ the region of active flow is given by $|Y| \leqslant P(\alpha T^{\alpha-1}X^3)^{1/7}$ and the total area covered by the flow is $|Y| \leqslant cX^{3\alpha/(4\alpha+3)}$, where P and c are constants. In the case $\alpha \geqslant 1$ the entire flow is active and the contact line is advancing at all points.

4.2. *Solutions near the contact line*

The long-time similarity solution of (2.12) satisfies

$$\alpha\phi = \frac{\partial}{\partial\xi}\left(\frac{4\alpha+3}{9}\xi\phi - \phi^3\right) + \frac{\partial}{\partial\eta}\left(\frac{\alpha}{3}\eta\phi + \phi^3\frac{\partial\phi}{\partial\eta}\right) \qquad (4.4)$$

in $|\eta| < \eta_{\rm P}(\xi)$, where $0 < \xi < \xi_{\rm N}$. From the definitions of the similarity variables, a fixed point (ξ, η) in similarity space represents a trajectory $YX^{-3\alpha/(4\alpha+3)}$ = constant in physical space. When the flow has entered the self-similar regime $T \gg 1$ it follows
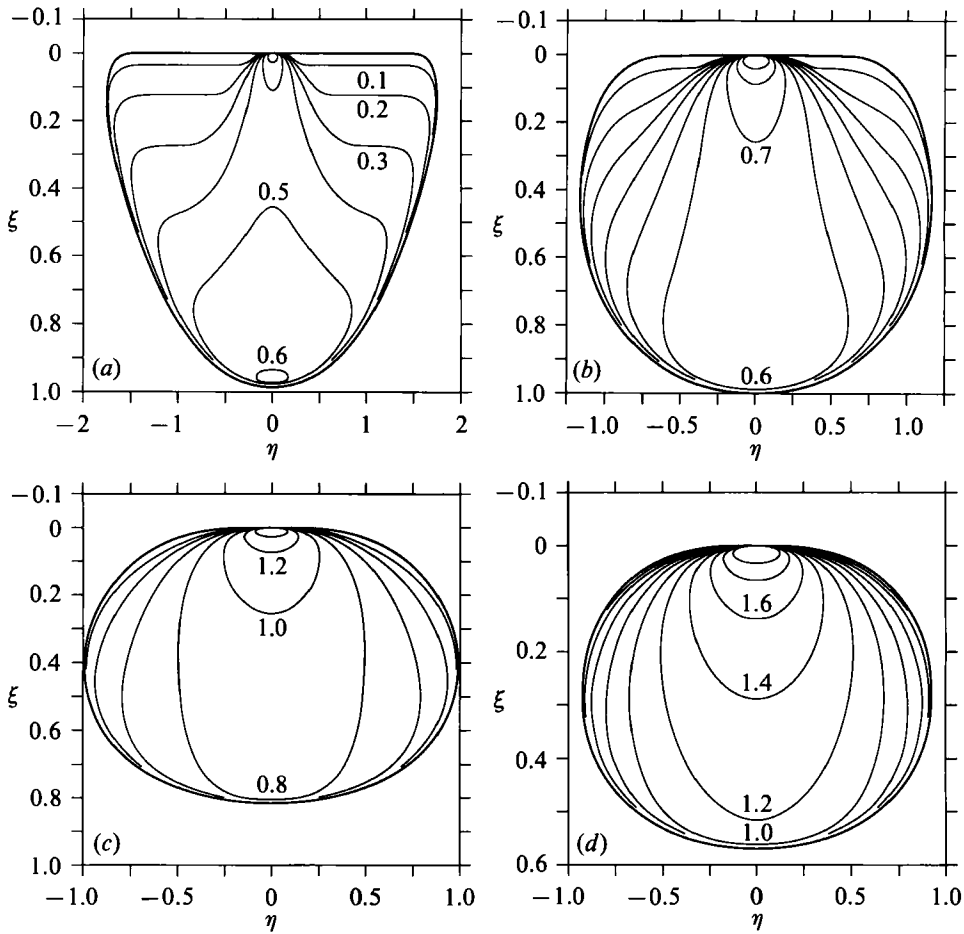
FIGURE 6. Contours of equal thickness in the similarity solutions of (4.4) for a flow of volume proportional to t^α from a point source on an inclined plane: (a) $\alpha = 0.05$, (b) $\alpha = 0.25$, (c) $\alpha = 1.0$, (d) $\alpha = 4.0$.

that a point $(\xi, \eta_P(\xi))$ on the perimeter of the flow represents an advancing contact line if

$$\frac{d\eta_P}{d\xi} < \left(\frac{3\alpha}{4\alpha+3}\right)\frac{\eta_P}{\xi}, \tag{4.5}$$

a stationary contact line if equality holds and a retreating contact line if the inequality is reversed. However, if surface forces are neglected, it is easily shown that a retreating contact line cannot occur within lubrication theory and so only the first two possibilities are relevant.

It is clear that the contact line is advancing near the downslope nose. From §4.1, the flow near the source is described by (4.1) and occupies a region that is shrinking if $\alpha < 1$ and growing if $\alpha > 1$. We may thus distinguish three cases. Firstly, if $0 < \alpha < 1$ the contact line is stationary in some region $\xi <$ constant, fixed at the 'high-water mark' it attained when the flow had been stronger. By integrating (4.5) with equality, we deduce that the stationary part of the contact line is described by $\eta_P \xi^{-3\alpha/(4\alpha+3)} =$ constant and hence only that part of the plane with $|y| \leqslant cx^{3\alpha/(4\alpha+3)}$ is eventually covered by the flow as $t \to \infty$, where c is a constant. The region between
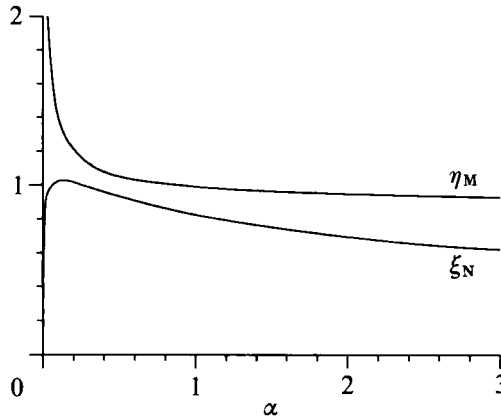
FIGURE 7. The coefficients of the dimensionless downslope and cross-slope extents, X_N and Y_M, of a viscous flow of volume T^α on an inclined plane in the long-time regime; $X_N \sim \xi_N T^{(4\alpha+3)/9}$ and $Y_M \sim \eta_M T^{\alpha/3}$ as $T \to \infty$. The singularity at $\alpha = 0$ represents the occurrence of powers of $\ln T$ in the similarity scaling for a fixed-volume release.

the stationary contact line and the asymptotic region of flow, given by (4.3) as $|Y| \leqslant P(\alpha T^{\alpha-1} X^3)^{\frac{1}{3}}$, is occupied by a thin draining film of fluid (figure 5). Secondly, if $\alpha = 1$ the contact line advances continually at all points but, at any fixed value of X, approaches the position given by the solution of (4.1). For $\mathcal{X} \gg 1$ this is given by $|Y| = P X^{\frac{2}{3}}$. Thus, for $\alpha = 1$ also, only part of the plane is eventually covered by the flow, but in this case the flow does not abate and there is no region covered by a thin draining film. Finally, if $\alpha > 1$ then the contact line advances continually at all points and all regions of the plane, upslope and downslope, are eventually covered by the flow.

For an advancing contact line where $\phi(\xi_P, \eta_P) = 0$ the leading-order terms in (4.4) are

$$\frac{(4\alpha+3)\,\xi_P}{9}\frac{\partial\phi}{\partial\xi} + \frac{\alpha\eta_P}{3}\frac{\partial\phi}{\partial\eta} + \frac{\partial}{\partial\eta}\left(\phi^3\frac{\partial\phi}{\partial\eta}\right) = 0. \qquad (4.6)$$

By resolving into coordinates normal and tangential to the contact line, it is readily shown that an appropriate solution of (4.6) only exists if $d\eta_P/d\xi$ is finite and satisfies (4.5). Moreover, when $-d\eta_P/d\xi \gg 1$ an extension of this analysis shows that the flow near the contact line has the boundary-layer structure (3.7) where χ is the normal distance from the contact line scaled by $(-d\eta_P/d\xi)^{-\frac{1}{2}}$ and ϕ_N is the thickness of the interior flow. Where $(-d\eta_P/d\xi)^{-\frac{1}{2}} \ll e^{-(\alpha+3)s/9}$ very close to the nose $(\xi_N, 0)$, the term $e^{-2(\alpha+3)s/9}(\phi^3\phi_\xi)_\xi$ in (2.12) must be retained to resolve the frontal shock structure (cf. the discussion in §3.2).

4.3. Numerical solutions

Numerical integration of (2.8) shows that the flow from a point source does indeed approach a long-time similarity solution described by (4.4). This solution is most easily calculated by integrating (2.12) to steady state with the exponentially small term neglected, as described in Appendix A. The numerical results, shown in figure 6 for a few values of α, confirm the local analyses given in §§4.2 and 4.3. In particular, the steep front of the profile for all values of α along the downslope portion of the contact line is striking. At small values of α the regions of active and draining flow are sufficiently large to be seen clearly. The values of ξ_N and η_M, shown in figure 7, allow the asymptotic extent of the current to be calculated, from which it is
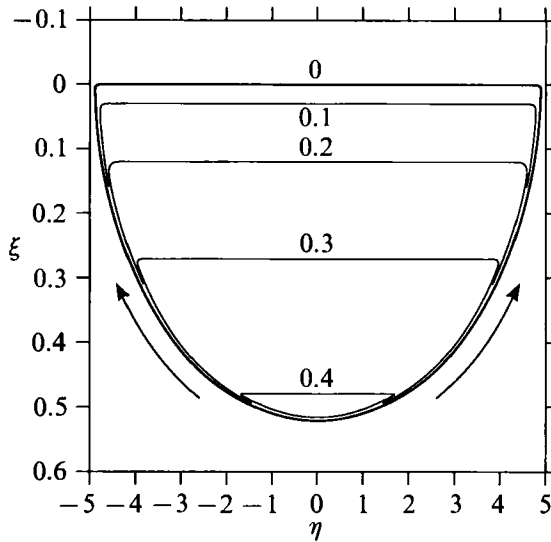
FIGURE 8. Contours of equal thickness in the numerical solution of (4.7) for the long-time evolution of a fixed-volume point release ($\alpha = 0$) at $s \approx 300$. The solution in the interior of the flow is given by $\phi \sim (\frac{1}{3}\xi)^{1/2}$; the flow continues to spread laterally as fluid is redistributed from the nose to the sides through the boundary layer at the edge of the flow.

straightforward to compare the theoretical prediction with experiments. The singularities in ξ_N and η_M as $\alpha \to 0$ reflect the result given below, that the dimensions of the flow are not described by a simple power-law in time in the case $\alpha = 0$.

4.4. *The case* $\alpha = 0$

Thus far we have concentrated on the case $\alpha > 0$. If we ignore the exponentially small terms in (2.12) for the case $\alpha = 0$ we obtain

$$\phi_s = (\tfrac{1}{3}\xi\phi - \phi^3)_\xi + (\phi^3\phi_\eta)_\eta \quad (\alpha = 0). \tag{4.7}$$

In this equation the outward diffusive flux $-\phi^3\phi_\eta$ in the η-direction cannot reach equilibrium since there is no balancing inward flux $-\tfrac{1}{3}\alpha\eta\phi$ as there was in (4.4.) for $\alpha \neq 0$. This suggests that the η-scale increases continually and there is no steady similarity solution in (ξ, η)-space.

As $s \to \infty$ the solution of (4.7) will satisfy $\xi_N \ll \eta_M$. A simple scaling argument shows that the terms involving η-derivatives are then much smaller than those involving ξ-derivatives through most of the flow. Hence the dominant balance in (4.7) is

$$(\tfrac{1}{3}\xi\phi - \phi^3)_\xi \sim 0 \tag{4.8}$$

with solution $\quad\quad\quad\quad \phi \sim (\tfrac{1}{3}\xi)^{\frac{1}{2}} \quad (|\eta| < \eta_P). \tag{4.9}$

Equation (4.8) is a singular perturbation of (4.7) and consequently (4.9) does not satisfy the boundary condition $\phi = 0$ on $\eta = \eta_P(\xi)$. Hence, we expect that there will be a thin boundary layer around the contact line in which the term involving η-derivatives is as important as those involving ξ-derivatives. The form of the interior solution (4.9) and the existence of such a boundary layer are confirmed by numerical integration of (4.7) (figure 8). The boundary layer carries a net lateral flux which redistributes fluid from the nose of the flow towards the sides. Detailed analysis of

(a)	Expt.	Fluid	Q (cm³ s⁻¹)	ν (cm² s⁻¹)	g' (cm s⁻²)	θ (°)	T^* (s)	X^*, Y^* (cm)	Symbol
	1	Silicone	1.48	11.3	981	2.5	38.2	10.9	○
	2	Silicone	1.48	11.3	981	5.0	9.5	5.4	△
	3	Silicone	1.48	11.4	981	10.0	2.4	2.7	●
	4	Glycerol	7.30	10.3	981	5.0	5.9	7.9	□
	5	Glycerol	8.40	8.4	981	5.0	5.0	7.8	×
	6	Glycerol	8.90	7.9	981	10.0	1.2	3.9	+
	7	Glycerol	31.30	7.4	981	5.0	3.2	10.5	■
	8	Glycerol	31.30	7.6	981	10.0	0.8	5.3	▲
	9	Syrup	0.23	35.4	262	10.5	21.7	3.0	□
	10	Syrup	0.34	36.0	262	14.3	10.7	2.4	●
	11	Syrup	0.77	173.5	301	10.5	47.5	5.8	○
	12	Syrup	2.09	34.6	262	17.5	4.3	3.1	△
	13	Syrup	2.09	34.6	262	17.5	4.3	3.1	■

(b)	Expt.	Fluid	Q (cm³)	ν (cm² s⁻¹)	g' (cm s⁻²)	θ (°)	T^* (s)	X^*, Y^* (cm)	Symbol
	14	Silicone	67	1.18	981	2.5	3.8	11.5	⌗
	15	Silicone	130	1.18	981	2.5	3.0	14.4	×
	16	Silicone	254	11.4	981	2.5	23.3	17.8	△
	17	Silicone	255	11.4	981	5.0	3.7	14.3	●
	18	Silicone	255	11.4	981	10.0	0.6	11.3	■
	19	Silicone	261	1.22	981	2.5	2.5	18.2	+
	20	Syrup	1770	250	981	9.7	7.1	21.8	□
	21	Syrup	1770	192	981	9.7	5.5	21.8	○
	22	Syrup	2327	36.6	981	9.7	1.0	23.9	▲

TABLE 2. The experimental parameters. The fluids used were silicone oil MS200/1000, two aqueous solutions of glycerol and a sugar syrup diluted with a little glycerol to make it less viscous. (*a*) Fixed-flux release; (*b*) Fixed-volume release.

this flux, given in Appendix B, allows the decrease in ξ_N and increase in η_M with s to be calculated. In physical space the results are

$$X_N \sim \left(\frac{3^{11}}{2^{10}(\ln T)^2}\right)^{\frac{1}{9}} T^{\frac{1}{3}}, \quad Y_M \sim \left(\frac{9 \ln T}{16}\right)^{\frac{1}{3}} \qquad (4.10)$$

as $T \to \infty$.

5. Experimental results

The theoretical solution (3.4) for downslope flow from a linear fixed-volume release has been verified experimentally by Huppert (1982*b*). As shown by (2.10*a*), the early-time behaviour of a point release on a slope is equivalent to axisymmetric spread on a horizontal surface. Huppert (1982*a*) derived a theoretical solution for spread in the latter situation and showed that it gave excellent agreement with experimental measurements. We now compare our long-time theoretical predictions for point release on a slope from constant-flux and constant-volume sources with the results of experiments. The data presented as Experiments 1–8 and 14–19 were very generously provided by M. A. Hallworth and H. E. Huppert. In both these experiments and our own the fluid viscosities and densities were determined by U-
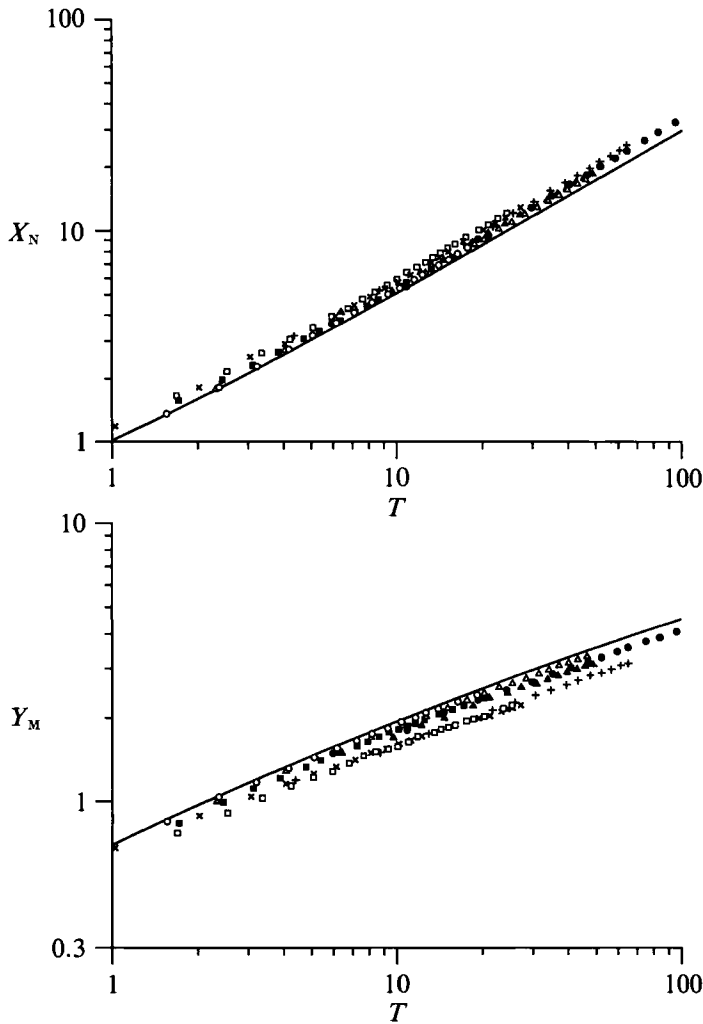
FIGURE 9. The dimensionless downslope and cross-slope extents, $X_N(T)$ and $Y_M(T)$, of viscous flows from a constant-flux point source in Experiments 1–8 and from solution of (2.8). The flows were all in air. The parameters and symbols used are summarized in table 2.

tube viscometer and hydrometer. The volumes and flow rates were then readily calculated from the mass of fluid released onto the slope. The experimental parameters are summarized in table 2. Measurements of the extent of the currents were either made directly or taken from photographs, using a ruled grid placed under the transparent inclined plane.

A series of experiments was conducted with a fixed-flux release from a constant-head reservoir onto an inclined glass plate about 1 m in length. The development of the downslope and cross-slope extent of the flows in eight of these experiments (Experiments 1–8) is shown in figure 9 normalized by the timescale T^* and lengthscales X^* and Y^* defined by (2.6). As suggested by the theory, these scalings collapse the data from the different experiments and the results are then seen to be in quite good agreement with a numerical solution of (2.8). The observed downslope extent is, however, systematically a little greater than predicted by the theoretical
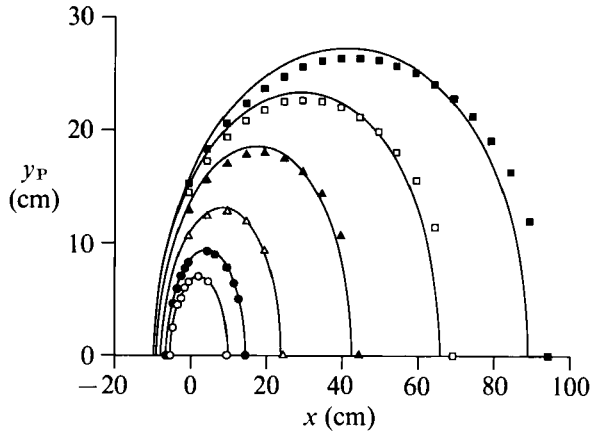
FIGURE 10. Measurements of the shape of a viscous flow from a constant-flux point source in Experiment 1, together with predictions obtained from numerical solution of (2.8). The shape is shown at 32 s (○), 59 s (●), 122 s (△), 271 s (▲), 486 s (□) and 727 s (■) after the initiation of the flow.

calculation and the cross-slope extent a little less than predicted. The same trend may be seen in figure 10 which compares the perimeter of the flow in Experiment 1 with the results of calculation at a number of times. Though the agreement is initially excellent, at later times the downslope flow is increased experimentally at the expense of the cross-slope flow.

Careful examination of these results, and those from some experiments at lower flow rates not shown in figure 10, shows that the difference between theory and experiment decreases with increasing flow rate and with decreasing surface tension[†] and is independent of the fluid viscosity. This strongly suggests that the difference may be ascribed to interfacial effects. As the flow thins and the buoyancy forces driving the cross-slope flow become weaker, surface-tension forces at the contact line will increasingly impede the cross-slope spread and hence channel the flow downslope.

In order to test this hypothesis, a series of experiments (Experiments 9–13) was conducted in which the viscous flow was established under water rather than in air. Viscous syrup was injected by a peristaltic pump at a constant flow rate through a hole in the sloping base of a Perspex tank filled with water. The syrup was miscible with water, more dense and much more viscous. In these experiments, therefore, interfacial forces were eliminated from the upper surface of the current and the flow should be described by (2.3) in which μ is the viscosity of the syrup and g is replaced by the reduced gravity $g' = g(\rho - \rho_w)/\rho$. It is thought that diffusion of water into the syrup was not significant on the timescale of the experiment. The results, shown in figure 11, are in good agreement with the theoretical predictions and do not display the systematic bias of the experiments conducted in air. We conclude that the analysis given in §§2 and 4 provides a good description of viscous flows on a slope where interfacial effects are absent or small.

Finally a series of experiments (Experiments 14–22) investigated the spread of a constant volume of fluid on a slope. In some of these experiments the fluid was initially held within a cylindrical barrier which was raised to commence the flow; in

[†] The coefficient of surface tension for glycerol is roughly three times that of silicone oil (Huppert 1982b).
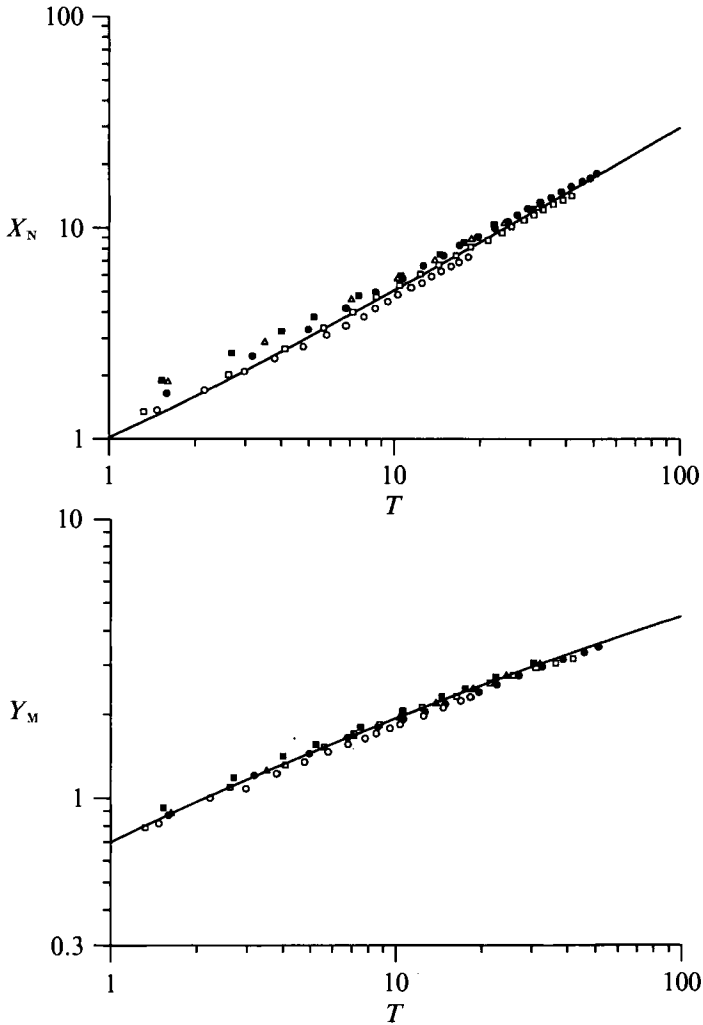
FIGURE 11. The dimensionless downslope and cross-slope extents, $X_N(T)$ and $Y_M(T)$, of viscous flows from a constant-flux point source in Experiments 9–13 and from solution of (2.8). The flows were all under water. The parameters and symbols used are summarized in table 2.

others the fluid was simply poured onto the plane during the first few seconds of the experiment. However, the method of release had very little effect on the subsequent flow. The scaled measurements of the extent of the current are shown in figure 12 together with the theoretical prediction obtained by integrating (2.8) numerically. The agreement is reasonably good, though, as for the constant-flux releases in air, there is a systematic tendency for the downslope extent to be larger and the cross-slope extent to be smaller in the experiment than the theory. Again, this is thought to be due to the influence of interfacial effects near the contact line.

In a few trial experiments with smaller volumes of fluid, the front of the current was observed to develop an instability which led to the formation and growth of a rivulet extending downslope from the nose (figure 13). This phenomenon was also observed by Huppert (1982b, figure 1b) and is due to the same capillary instability that causes the front of a two-dimensional current to break into a series of rivulets
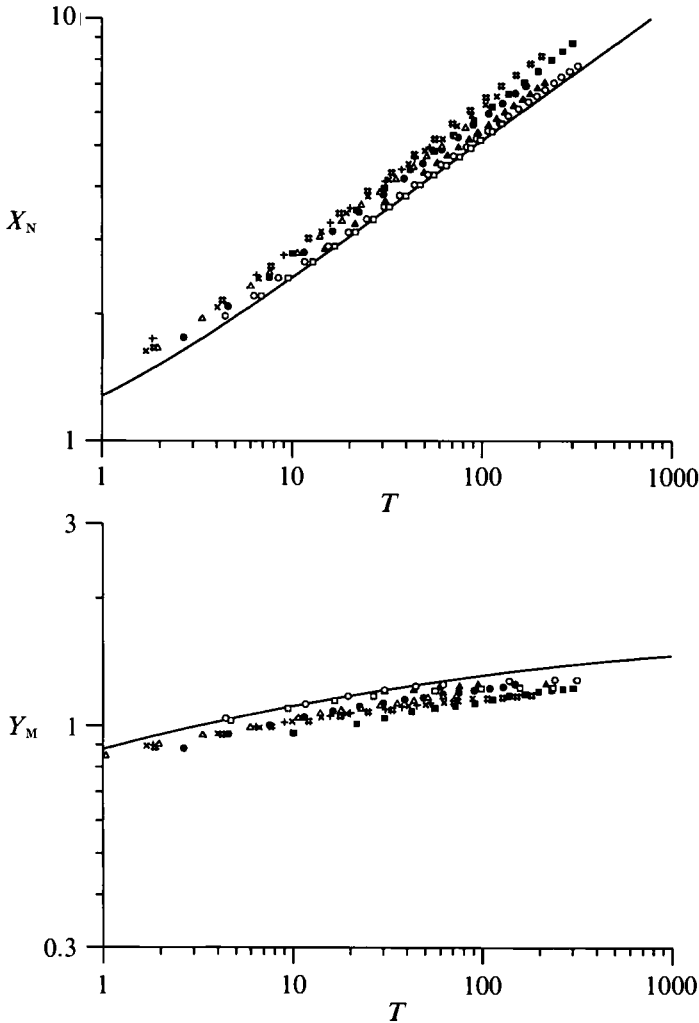
FIGURE 12. The dimensionless downslope and cross-slope extents, $X_N(T)$ and $Y_M(T)$, of viscous flows from a constant-volume release in Experiments 14–22 and from solution of (2.8). The flows were all in air. The parameters and symbols used are summarized in table 2.

(Huppert 1982b, figures 1c–g). By observing the appearance of perturbations to the previously straight front of the two-dimensional current, Huppert was able to show that the onset of instability occurred when the length of the current was proportional to the square root of its volume. However, in the present case, in which the contact line is curved even before instability, it was not possible to locate the onset of instability with sufficient precision to identify an instability criterion, though it is clear that instability occurs later if the volume of the current is increased.

6. Discussion

We have analysed the flow of viscous fluid on a slope using lubrication theory and derived solutions for the shape and rate of spread of the current. These solutions are found to give very good agreement with experimental observations provided that surface tension and contact-line effects are dominated by buoyancy and the flow is
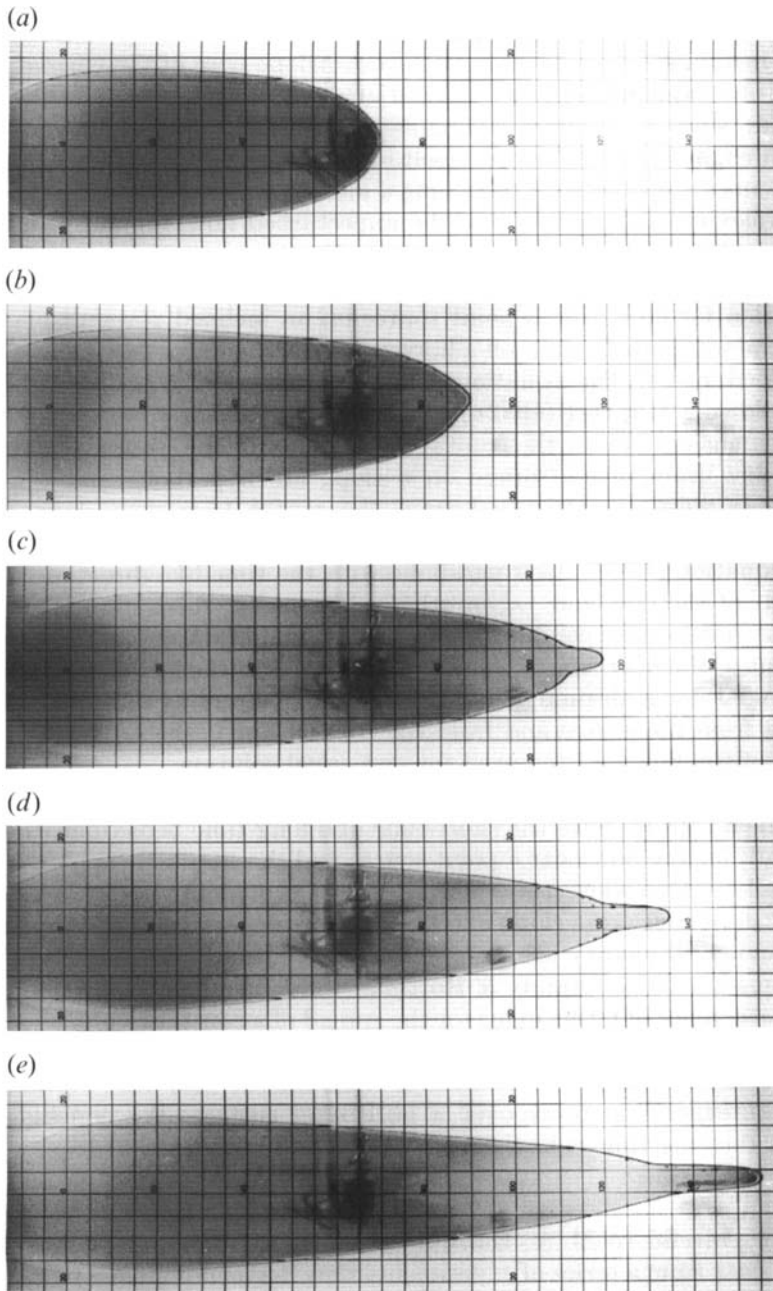
FIGURE 13. The development of a capillary rivulet at the downslope nose of a fixed-volume flow of syrup on an inclined Perspex plane. The photographs are at (a) 160 s, (b) 280 s, (c) 440 s, (d) 580 s and (e) 720 s after the initiation of the flow and the capillary instability seems to occur near the time of (b). The grid spacing is 5 cm and the volume of the flow is about 550 cm³.

governed by a simple viscous–buoyancy balance as envisaged by the theory. This will indeed be the case if the viscous flow is miscible with its surroundings or if the volume of the flow is sufficiently large, for example, as in geological applications (Huppert *et al.* 1982; Kerr & Lister 1987).

When interfacial forces do play a role, they inhibit cross-slope spread, channelling the flow downslope. At very long times, when the current is thin and slowly moving, a capillary instability may develop at the downslope nose of the current, leading to the growth of a capillary rivulet. Detailed analysis of these effects is likely to prove very difficult since it involves a singular perturbation of the viscous–buoyancy balance, which, as has been shown, itself involved a number of subtleties. Thus the usual problems associated with modelling a moving contact line will be compounded by the complexity of the solution of the unperturbed flow. Similarly, it may prove difficult to analyse the consequences of a non-Newtonian or temperature-dependent viscosity as a model, for example, of a solidifying lava flow.

The solution for flow from a point source on an inclined plane displays features from both the solutions for flow on a horizontal plane and for flow from a line source on an inclined plane. The equations describing flow on a horizontal surface are parabolic allowing Huppert (1982a) to obtain a similarity solution by integrating from an expansion about the contact line toward the source. The equations describing flow from a line source on a slope are hyperbolic and the similarity equation (3.1) must be integrated from the source to a downslope shock. The equation governing long-time flow from a point source is mixed in type, and the similarity equation (4.4) is itself parabolic with the time-like direction being $+\xi$ in some regions of the flow and $-\xi$ in others. Physically, this shows that the flow is influenced by both source conditions and the location of the contact line. The former are dominant in the near-source solution (4.3), whereas the latter is dominant in the regions covered by a draining film ($\alpha < 1$). This interplay between information propagating from the source and from the contact line is the origin of much of the complexity of the flow and the need for numerical solution.

Some features of the results are pleasantly simple. These include the scalings (2.6) and (2.7) which capture both the short-time and long-time behaviour, the universal structure (4.3) for the flow near a point source and the simple form $|y| < cx^{3\alpha/(4\alpha+3)}$ of the area finally wetted when $0 < \alpha \leqslant 1$. However, though the power-law dependence of the downslope and cross-slope extent of the flows with $\alpha > 0$ is similar to that found in previous similarity solutions for gravity currents in other situations (Fay 1969; Buckmaster 1973; Grundy & Rottman 1986; Huppert 1982a; Lister & Kerr 1989), the occurrence of terms in $\ln t$ for the spread of a constant volume of fluid from a point source is somewhat unexpected. The local non-uniformities in the asymptotic similarity solution at the steep downslope front and at thin draining films upslope have no counterparts in flows over a horizontal surface. We conclude that the solutions for the long-time behaviour of flows on an inclined plane display surprising structure.

Appendix A. The numerical scheme

Numerical solutions to (2.8), (4.1), (4.4) and (4.7) were computed using a finite-difference scheme on a rectangular grid. The equations were written in flux-conservative form and the spatial derivatives in the advective and diffusive terms were represented by the Il'in scheme, which combines centred and upwind differencing (Il'in 1969; Clauser & Kiesner 1987). In the cases of (4.4) and (4.7) a small amount of numerical viscosity in the ξ-direction was added to smooth spatial oscillations at the downslope shock. Time-stepping was performed using an alternating-direction-implicit method, with evaluation of the non-constant coefficients at the midpoint of the time-step. The discretization was thus second-order accurate in both space and time, and differs from that used by Schwartz & Michaelides (1988) and Schwartz (1989) primarily in the treatment of the spatial derivatives. The accuracy of the solutions was checked by comparison with the analytic solutions of Smith (1973) and Huppert (1982a), by grid refinement, and, where applicable, by variation of the amount of artificial viscosity.

Appendix B. The long-time solution for $\alpha = 0$.

In §4.4 we argued that the solution of (4.7) approaches a quasi-steady state in which the interior solution (4.9) is matched to a boundary layer which slowly redistributes fluid around the perimeter of the flow from the nose to the sides. As a result, ξ_N decreases and η_M increases with s as the shape of the flow evolves in (ξ, η)-space. We now show that as $s \to \infty$ the flow occupies the region $0 \leqslant \xi \leqslant \xi_P$, where ξ_P is of the form

$$\xi_P(\eta, s) = \xi_N(s) f\left(\frac{\eta}{\eta_M(s)}\right) \quad (-\eta_M \leqslant \eta \leqslant \eta_M) \tag{B 1}$$

and $\xi_N(s)$, $\eta_M(s)$ and f are functions which are determined by consideration of the flux in the boundary layer.

The structure of the boundary layer is obtained by transformation into coordinates which are locally tangential and normal to the contact line at $(\xi_P(\eta, s), \eta)$. We find that the leading-order approximation of (4.7) within the boundary layer is given by

$$(\tfrac{1}{3}\xi_P\phi - \phi^3)' = (\partial\xi_P/\partial\eta)^2(\phi^3\phi')', \tag{B 2}$$

where primes denote differentiation with respect to the normal coordinate. This equation is of the same form as (3.6), showing that the boundary-layer profile is given by (3.7), where $\phi_N = (\tfrac{1}{3}\xi_P)^{\frac{1}{2}}$ and χ is the distance from the contact line scaled by the boundary-layer width $\delta = \phi_N(\partial\xi_P/\partial\eta)^2$. We note that $\delta \ll \xi_P$ since $\partial\xi_P/\partial\eta \ll 1$ as $s \to \infty$. Hence, the variation of ϕ across the boundary layer is much greater than that along the boundary layer, and the contours of ϕ within the boundary layer are nearly parallel to the contact line. It follows that the total flux in the η-direction is given by

$$F(\eta, s) = \int \phi^3\phi_\eta \, d\xi \sim \frac{\partial\xi_P}{\partial\eta} \int \phi^3\phi_\eta \, d\eta = -\frac{\partial\xi_P}{\partial\eta}\frac{\phi_N^4}{4}, \tag{B 3}$$

where the integrals are taken along a contour crossing the boundary layer.

Owing to this lateral flux, the region occupied by the interior solution evolves with time. By substituting (4.9) and (B 1) into the volume constraint $\int\phi = 1$, we obtain

$$2\eta_M(\tfrac{1}{3}\xi_N)^{\frac{3}{2}} \int_{-1}^{1} \{f(u)\}^{\frac{3}{2}} \, du = 1, \tag{B 4}$$

showing that $\eta_M \xi_N^3$ is constant. Now, by conservation of volume, $F(\eta', s)$ is equal to the rate of decrease of the volume in $0 < \eta < \eta'$. Thus from (B 1)

$$F(\eta, s) = -\frac{\partial}{\partial s}\left(2\eta_M(\tfrac{1}{3}\xi_N)^{\frac{3}{2}}\int_0^{\eta/\eta_M(s)}\{f(u)\}^{\frac{3}{2}}\,\mathrm{d}u\right) = 2\eta(\tfrac{1}{3}\xi_P)^{\frac{3}{2}}\left(\frac{\dot{\eta}_M}{\eta_M}\right), \qquad \text{(B 5)}$$

where the dot denotes differentiation with respect to s.

We equate the expressions (B 3) and (B 5) for the flux F and integrate with respect to η to obtain

$$(\tfrac{1}{3}\xi_P)^{\frac{3}{2}} + 2\eta^2(\dot{\eta}_M/\eta_M) = c(s), \qquad \text{(B 6)}$$

where the integration constant $c(s)$ is determined by (B 4). We conclude that the long-time solution of (4.7) is given by the interior solution (4.9) matched to the boundary-layer profile (3.7) along the perimeter (B 1), where

$$f(u) = (1 - u^2)^{\frac{3}{4}}, \quad \xi_N = \left(\frac{3^{11}}{2^{10}s^2}\right)^{\frac{1}{6}} \approx 1.773\,s^{-\frac{2}{9}}, \quad \eta_M = \left(\frac{9s}{16}\right)^{\frac{1}{3}} \approx 0.825\,s^{\frac{1}{3}}. \quad \text{(B 7}a\text{–}c\text{)}$$

These results have been verified numerically. There is a small region near $\eta = \eta_M$ where $\partial\xi_P/\partial\eta$ is not small and the boundary-layer analysis given here breaks down. However, this region has no effect on the asymptotic evolution of the rest of the flow.

REFERENCES

BUCKMASTER, J. 1973 Viscous-gravity spreading of an oil slick. *J. Fluid Mech.* **59**, 481–491.

CLAUSER, C. & KIESNER, S. 1987 A conservative, unconditionally stable, second-order, three-point differencing scheme for the diffusion-convection equation. *Geophys. J. R. Astr. Soc.* **91**, 557–568.

FAY, J. A. 1969 The spread of oil slicks on a calm sea. In *Oil on the Sea* (ed. D. P. Hoult), pp. 53–63. Plenum.

GOODWIN, R. & HOMSY, G. M. 1991 Viscous flows down a slope in the vicinity of a contact line. *Phys. Fluids* A **3**, 515–528.

GRUNDY, R. E. 1983 Asymptotic solutions of a model nonlinear convective diffusion equation. *IMA J. Appl. Maths* **31**, 121–137.

GRUNDY, R. E. & ROTTMAN, J. W. 1986 Self-similar solutions of the shallow-water equations representing gravity currents with variable inflow. *J. Fluid Mech.* **169**, 337–351.

HOCKING, L. M. 1990 Spreading and instability of a viscous fluid sheet. *J. Fluid Mech.* **211**, 373–392.

HUPPERT, H. E. 1982*a* The propagation of two-dimensional and axisymmetric viscous gravity currents over a rigid horizontal surface. *J. Fluid Mech.* **121**, 43–58.

HUPPERT, H. E. 1982*b* Flow and instability of a viscous current down a slope. *Nature* **300**, 427–429.

HUPPERT, H. E., SHEPHERD, J. B., SIGURDSSON, H. & SPARKS, R. S. J. 1982 On lava dome growth, with application to the 1979 lava extrusion of Soufriére, St Vincent. *J. Volcanol. Geotherm. Res.* **14**, 199–222.

IL'IN, A. M. 1969 Differencing scheme for a differential equation with a small parameter affecting the highest derivative. *Math. Notes Acad. Sci. USSR* **6**, 596–602.

KERR, R. C. & LISTER, J. R. 1987 The spread of lithospheric material along the mid-mantle boundary. *Earth Planet. Sci. Lett.* **85**, 241–247.

LISTER, J. R. & KERR, R. C. 1989 The propagation of two-dimensional and axisymmemtric viscous gravity currents along a fluid interface. *J. Fluid Mech.* **203**, 215–249.

SCHWARTZ, L. W. 1989 Viscous flows down an inclined plane: Instability and finger formation. *Phys. Fluids* A **1**, 443–445.

SCHWARTZ, L. W. & MICHAELIDES, E. E. 1988 Gravity flow of a viscous liquid down a slope with injection. *Phys. Fluids* **31**, 2739–2741.

SILVI, N. & DUSSAN V., E. B. 1985 On the rewetting of an inclined solid surface by a liquid. *Phys. Fluids* **28**, 5–7.

SMITH, P. C. 1973 A similarity solution for slow viscous flow down an inclined plane. *J. Fluid Mech.* **58**, 275–288.

TROIAN, S. M., HERBOLZHEIMER, E., SAFRAN, S. A. & JOANNY, J. F. 1989 Fingering instabilities of driven spreading films. *Europhys. Lett.* **10**, 25–30.